Can bi-functional nickel modified 13X and 5A zeolite catalysts for CO_2 methanation be improved by introducing ruthenium?

Wei, Liangyuan; Kumar, Narendra; Haije, Wim; Peltonen, Janne; Peurla, Markus; Grénman, Henrik; de Jong, Wiebren

DOI
10.1016/j.mcat.2020.111115

Publication date
2020

Document Version
Final published version

Published in
Molecular Catalysis

Molecular Catalysis 494 (2020) 111115

Contents lists available at ScienceDirect

Molecular Catalysis

journal homepage: www.elsevier.com/locate/mcat

Can bi-functional nickel modified 13X and 5A zeolite catalysts for CO_2 methanation be improved by introducing ruthenium?

Liangyuan Wei[a], Narendra Kumar[b], Wim Haije[a], Janne Peltonen[c], Markus Peurla[d], Henrik Grénman[b,*], Wiebren de Jong[a,*]

[a] Faculty 3mE, Department of Process and Energy, Section Large-Scale Energy Storage, Delft University of Technology, Delft, the Netherlands
[b] Faculty of Science and Engineering, Johan Gadolin Process Chemistry Centre, Laboratory of Industrial Chemistry and Reaction Engineering, Åbo Akademi University, Turku/Åbo, Finland
[c] Department of Physics and Astronomy, University of Turku, Turku, Finland
[d] Institute of Biomedicine, University of Turku, Finland

ARTICLE INFO

Keywords:
Ni and Ru
13X and 5A zeolite catalysts
CO_2 methanation

ABSTRACT

Zeolites 13X and 5A were modified with nickel and/or ruthenium for CO_2 methanation. The catalysts were prepared by evaporation impregnation and XRD, SEM-EDX, TEM, STEM-EDX, nitrogen physisorption, H_2-TPR and NH_3-TPD were used to characterize the physico-chemical properties of the catalysts. The physico-chemical characterization results show that the zeolites structure did not change after the Ni, Ru modification, however. Ni was able to enter the pores of 13X, in the other case, 5A, an egg shell type structure was formed. Methanation experiments were performed in a lab scale fixed bed reactor system, the results showed that the mono-metallic catalysts out-performed the bi-metallic ones with Ni being the more active. One of the factors influencing the performance of the bi-metallic catalysts was the difficulty to obtain good dispersion when both metals were used. Also the morphology of the catalyst significantly influenced the selectivity. The catalysts with lower weak acidity benefit for getting a higher activity. The single metal catalysts 2.5 %Ru13X and 5%Ni13X showed good catalytic stability with around 97 % CH_4 selectivity at 360 °C, with no catalyst deactivation during the 200 h catalyst stability test.

1. Introduction

Hydrogen energy is regarded as one of the most potential clean energy sources in 21 st century. It can be produced from carbon fuels conversion like biomass gasification [1,2], or made from electricity and water, however, it is difficult to store and dangerous to transport, especially on a large scale [3]. These challenges limit the transition to a hydrogen economy [4]. Simultaneously, global warming is one of the most important environmental issues and the greatest challenges facing humanity today. Carbon dioxide is one of the most important greenhouse gases emitted on large scale from fossil fuel combustion processes. One of the methods for tackling these challenges is to capture CO_2 e.g. from stack sources and perform methanation with renewable H_2 via the Sabatier reaction ($CO_2 + 4H_2 \leftrightarrow CH_4 + 2H_2O$; $\Delta H^0_{298} = -165$ kJ/mol) [5–7]. The product methane fits directly into existing energy infrastructure, and can easily be liquefied and transported.

In order to meet the gas grid requirement for substitute gas high purity is required, however, this requires an significant shift of the equilibrium (for high conversion) i.e. practically the removal of water [8,9]. These results show that there is clear benefit to be gained by having the water sorption properties in close vicinity of the active metals. This can be achieved by sequential reaction-separation steps in e.g. alternating fixed bed reactors [9]. However, a more elegant and most probably economic alternative would be combining these functions, the catalytic and adsorptive, into a single bi-functional catalyst. Delmelle et al. studied the sorption enhanced methanation of CO_2 by loading Ni on zeolite 5A and 13X with wet impregnation and, they found that Ni/zeolite catalysts have a high activity and selectivity in CO_2 methanation [10]. Borgschulte et al. modified zeolite 5A by Ni, and observed a significant sorption enhanced effect in CO_2 methanation [11]. Methanation has been studied with different metals based catalysts, such as Ru, Ir, Rh and Ni [7,12–17]. Ni based catalysts are the most widely used due to their rather high activity, CH_4 selectivity and low cost [8,18–21]. Ru is known to be more active compared to Ni, with also high CH_4 selectivity and low coke forming properties [12,22]. From the adsorption point of view, zeolites 13X and 5A are known for

* Corresponding authors.
E-mail addresses: henrik.grenman@abo.fi (H. Grénman), Wiebren.deJong@tudelft.nl (W. de Jong).

https://doi.org/10.1016/j.mcat.2020.111115
Received 28 February 2020; Received in revised form 5 June 2020; Accepted 6 July 2020
Available online 28 July 2020

their high water-uptake properties [10,11,23].

The current project focuses on synthesis of bi-functional material possessing both catalytic and water adsorptive properties by depositing nickel and/or ruthenium on zeolites 13X and 5A using evaporation impregnation. The aim in the current work was the comparison of catalytic activities of the synthesized monometallic Ni and Ru catalysts with the bi-metallic Ni/Ru catalysts with varying proportions of the metals excluding the sorption enhancement. The high activity of Ru at low temperature could be beneficial for the sorption enhanced CO_2 methanation. Surprisingly, the combination of Ru and Ni is hardly mentioned in sorption enhanced methanation literature, therefore, Ru combined with Ni on 13X and 5A zeolite were synthesized, characterized and tested for CO_2 methanation.

In this paper, 5%Ni13X, 1%Ru4%Ni13X, 2.5 %Ru2.5 %Ni13X, 2.5 %Ru13X, 5%Ni5A, 1%Ru4%Ni5A, 2.5 %Ru2.5 %Ni5A, 2.5 %Ru5A zeolite catalysts were prepared by evaporation impregnation. The pH of the solution during the preparation of each catalyst was monitored by pH meter. After the catalyst were prepared, XRD, SEM-EDX, TEM, STEM-EDX, nitrogen physisorption and H_2-TPR were used for physico-chemical characterization of crystal structure, morphology, NiO particle size, surface area and pore volume. Additionally, NH_3-TPD was used to determine the acidity of catalysts. The activity and selectivity tests of catalysts were carried out in a laboratory scale fixed bed reactor system (Fig. S. 1, Supplementary material).

2. Experimental

2.1. Catalyst preparation using evaporation impregnation, deposition precipitation and ion-exchange methods

The catalyst 5%Ni13X, 1%Ru4%Ni13X, 2.5 %Ru2.5 %Ni13X, 2.5 % Ru13X, 5%Ni5A, 1%Ru4%Ni5A, 2.5 %Ru2.5 %Ni5A and 2.5 %Ru5A were prepared by evaporation impregnation method. A Ni-, Ru-, metal loading of 5% was targeted on the 13X and 5A zeolite supports. Nickel nitrate hexahydrate ($Ni(NO_3)_2{\cdot}6H_2O$, 99 %, Merck Millipore) and Ruthenium (III)-chloride hydrate ($RuCl_3{\cdot}xH_2O$, 99 %, Aldrich) were used as the Ni and Ru precursors. The metal precursors were dissolved in 250 mL of distilled water in a flask, and 5 g of $0.212-0.500$ mm size (sieved fraction and dried at 100 °C overnight in an oven) 13X zeolite (Honeywell Fluka, The Netherlands) or 5A zeolite (Merck Millipore, The Netherlands) was added to the solution. The pH of the solution was measured by a pH meter during this process. In order to avoid the mechanical wear of zeolite, the rotator evaporator was operated at low rotation speed, 10 rpm, for 24 h at room temperature. After 24 h of catalyst synthesis, evaporation of the aqueous solution was carried out in the rotator evaporator at 50 °C using a water jet pump. The catalyst was dried at 100 °C overnight in an oven before calcination.

All catalysts were calcined in a muffle furnace using a step calcination procedure. In the stepwise calcination procedure, the heating rate from room temperature to 250 °C was 4.5 °C/min, where it was kept for 40 min, after which the temperature was increased to the target temperature (e.g. 400 °C) by 2.5 °C/min, where it was kept for 3 h and then cooled down to room temperature.

2.2. Catalyst characterization

The calcined catalysts were characterized before reduction by X-ray powder diffraction (XRD), scanning electron microscopy (SEM), transmission electron microscopy (TEM), scanning transmission electron microscopy equipped with an energy-dispersive X-ray spectroscopy (STEM-EDX), nitrogen physisorption, hydrogen temperature programed reduction (H_2-TPR), and temperature programmed ammonia desorption (NH_3-TPD).

The PANalytical Empyrean X-ray powder diffractometer was used in the XRD measurements. The diffractometer was operated in Bragg-Brentano diffraction mode, and the monochromatized Cu-$K\alpha$ radiation ($\lambda = 1.541874$ Å) was generated with a voltage of 45 kV and a current of 40 mA. The measured XRD diffractograms were analyzed with Philips X'Pert HighScore (phase analysis refinement) and MAUD programs (background subtraction), and the scanning 2θ angle range was 3.0° to 80.0° by step size of 0.013°, counting time 80 s/step.

Catalysts morphology, shape, size and distributions of crystals were studied by scanning electron microscopy (SEM) LEO Gemini 1530 (LEO/ZEISS, Germany). The catalyst elemental analysis was carried out by energy dispersive X-ray spectroscopy (EDX).

Transmission electron microscopy (TEM) was used to study the Ni-, Ru- particle size and distributions. The average RuO_2 or NiO particle size was calculated. Furthermore structure, textural properties of the pristine 13X and 5A zeolites and Ru-, Ni- modified 13X and 5A catalysts were also investigated using transmission electron microscopy. The equipment used was JEM-1400 (JEOL Itd, Japan) which maximum acceleration voltage is 120 kV.

To further study the composition and the nanoscale structure of the catalysts, scanning transmission electron microscopy equipped with an energy-dispersive X-ray spectroscopy (STEM-EDX) detector was used. The equipment used was FEI Titan 80–300 electron microscope, the elemental mapping was investigated at a voltage of 300 kV with EDX. Specimen preparation consisted of immersing a lacey carbon film supported on a copper grid into the catalysts powder, small particles adhering to the carbon film were measured.

The surface area, pore size and pore volume of pristine 13X and 5A zeolite, Ni-, Ru- modified 13 X and 5A zeolite catalysts were measured by nitrogen adsorption. The instrument used was 3Flex Physisorption (Micromeritics Instrument Corp.). The calculation of surface area was carried out using the BET method. The catalysts were outgassed at 350 °C for 3 h, prior to the surface area measurement.

H_2-TPR analysis was carried out in a Micromeritics AutoChem 2910. The catalysts were dried at 250 °C for 1 h with dry Ar atmosphere, then reduced by 5% H_2 (diluted by Ar) from room temperature to 900 °C with 5 °C/min heating rate, a TCD detector was used to monitor the H_2 consumption.

Temperature programmed desorption was carried out in Micromeritics AutoChem 2910 to investigate the acidity of the catalysts, the samples were dried at 250 °C for 0.5 h with dry He atmosphere before ammonia adsorption (5% NH_3 diluted by He) at room temperature, the desorption temperatures were from 100 to 900 °C.

2.3. Catalyst test

The prepared catalyst activity, selectivity and stability were tested in a fixed bed reactor system (Fig. S. 1, Supplementary material), made of quartz reactor with an inner diameter of 10 mm. Silica beads (around 10 mL) were placed in the lower part of the reactor to support the catalyst bed then, silica beads and the catalyst were layered by quartz wool, and silica beads (around 10 mL) were used again to fill the reactor. The reactor was heated by a vertical tube furnace equipped with a K-type thermocouple, while the temperature of the catalyst bed was monitored by another K-type thermocouple which was inserted into the bottom of catalyst bed and connected to the computer for recording and showing. A schematic of the fixed bed reactor system can be found in Fig. S. 1 (Supplementary material).

In the catalyst test, 0.9 g of catalyst was loaded into the reactor and reduced under 100 mL/min H_2 atmosphere at 500 °C for 4 h. Catalysts activity experiments were performed at 240 °C–440 °C with a gas hourly space velocity of 13333 mL/g_{cat}/h, in reaction, 40 mL/min H_2 and 10 mL/min CO_2 diluted by N_2 (150 mL/min). The product gas from the reactor was lead through a cooling condenser and then analyzed by GC (Varian, CP-4900 Micro-GC). Helium was used as the carrier gas.

The CO_2 conversion (1) and catalyst selectivity (2) for CH_4 are defined as [24,25]:

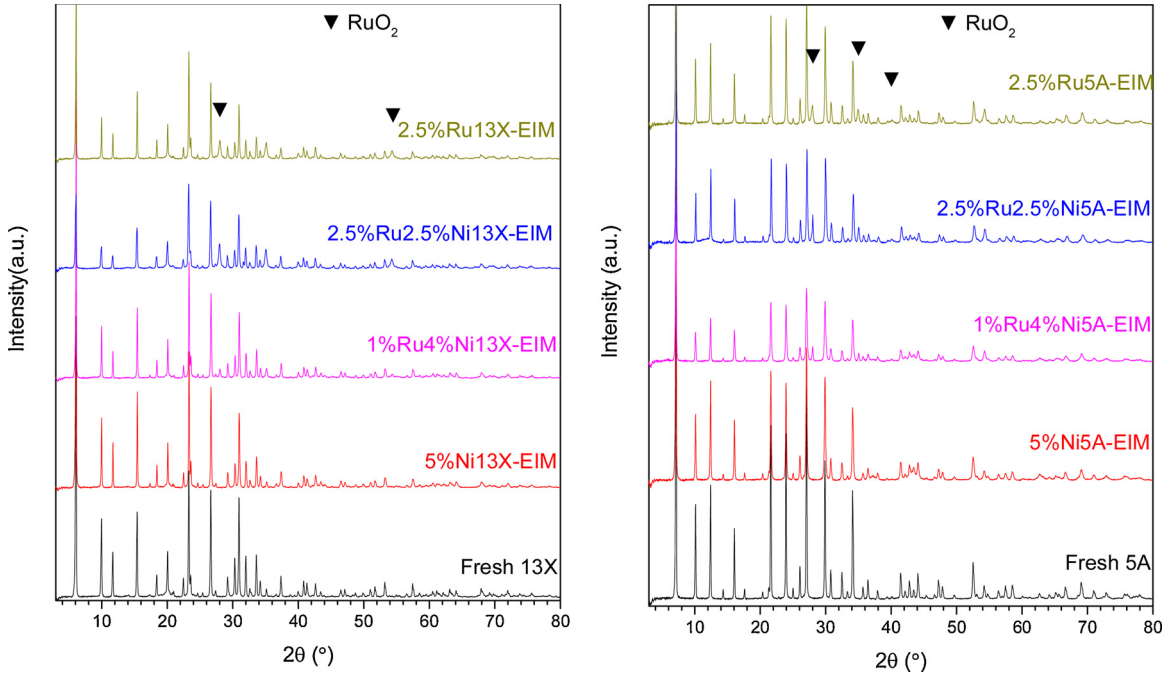

Fig. 1. X-ray powder diffraction patterns for Ni or Ru13X and 5A zeolite catalysts, fresh 13X and 5A zeolite.

$$X_{CO_2} = \frac{n_{CO_2,\,in} - n_{CO_2,\,out}}{n_{CO_2,\,in}} \quad (1)$$

$$S_{CH_4} = \frac{n_{CH_4,\,out}}{n_{CO_2,\,in} - n_{CO_2,\,out}} \quad (2)$$

Where n_{CO_2} is the input molar flow rate of CO_2 in experiment, $n_{CO_2,\,out}$, $n_{CH_4,\,out}$ are the molar flow rate of CO_2 and CH_4 calculated from GC results, respectively (selectivity < 100 % means CO is formed).

3. Results and discussion

3.1. Catalyst characterization results

3.1.1. X-ray powder diffraction

The crystal structure of the Ni modified catalysts 5%Ni13X, 5% Ni5A, Ni and Ru modified 13X and 5A zeolite, fresh 13X and 5A zeolite were investigated by XRD measurement. As in Fig. 1, the X-ray powder diffraction patterns indicated that catalyst preparation did not influence the crystal structure of 13X and 5A zeolites. Additionally, the peaks of RuO_2 for Ru modified 13X zeolite and 5A were observed from the XRD peaks, while the peaks for NiO could not be identified in the X-ray powder diffraction patterns (Fig. 1). The plausible explanation for this observation could be the peak broadening due to lowercrystallinity as well as small nanoparticle size in the lower end of the particle size distribution (0.72–28.23 nm) (Table S. 4).

3.1.2. Scanning electron microscopy (SEM) and Energy dispersive X-ray spectroscopy (EDX)

The morphology of Ni and Ru modified catalysts were investigated by SEM, as shown in Fig. 2. The 13X zeolite showed large crystals (around 2 μm) composed of small fibrous crystals [10], less visible in 1%Ru4%Ni13X and 2.5 %Ru2.5 %Ni13X (Fig. 2). The small fibrous crystals of fresh 13X and 5%Ni13X are much more visible than in 1% Ru4%Ni13X and 2.5 %Ru2.5 %Ni13 × . This may be due to change of fibrous crystals during the catalyst preparation, due to the acidic pH of Ruthenium (III)-chloride aqueous solution. The pH of the solution decreased dramatically from 6.69 to around 2.32 (Table S. 2, Supplementary material), when ruthenium chloride was dissolved in the solution, while it increased to 4.13 after 13X zeolite was introduced. The increase in the pH of the ruthenium chloride solution after addition of 13X zeolite was attributed to the adsorption of ruthenium by 13 × . The pH of solution was the lowest in the preparation of 2.5 %Ru2.5 % Ni13X and 2.5 %Ru13X catalysts. By contrast, the pH of the solution was around 7.5 during the preparation of 5%Ni13 × . The enhanced pH of the 5%Ni13X catalyst synthesis solution is attributed to the higher pH (7.4) of Ni $(NO_3)_2$ solution as compared to highly acidic pH (2.1) of $RuCl_3$ solution (Table S 2).

Fresh 5A zeolite shows the smoothest crystal surface. The honeycomb type architecture of the 5A zeolite crystal surface could be NiO crystals, which displayed only on the Ni modified 5A zeolite surface.

In order to investigate the chemical composition of samples as well as the actual loading of Ni and Ru is in the Ni-, Ru-13X and 5A zeolite catalysts, SEM combined with EDX was employed. It was observed that Si to Al ratio in 13X and 5A zeolite did not change during the Ni, Ru modification (Table S. 3, Supplementary material). This is consistent with the XRD results (Fig. 1), which also show that the zeolite structure was maintained during modification.

3.1.3. Transmission electron microscopy (TEM)

The NiO particle size, distribution and morphology were analyzed with transmission electro micrographs (TEM). The images show the typical uniform porous structures of the 13X and 5A zeolite along with Ni and Ru nanoparticles. A small average NiO particle size around 10 nm can be observed for both 5%Ni13X and 5%Ni5A catalysts (Fig. 3). However, the distribution of the particle size ranges from well below one nm upwards (Table S. 4) and the smallest particles are difficult to detect due to limitations of the analysis method. The results indicate that some of the Ni is located inside the pores of the 13X zeolite, however, the larger particles are clearly located on the external surface of the zeolite particles.

The RuO_2 was not well dispersed and displayed significantly larger average nanoparticle size and also the smallest detected particles were considerably larger than for Ni. RuO_2 appeared as big nanoparticles with a particle size range 7.3–97.7 nm (average 37.5 nm) for 2.5 % Ru13 × . The average RuO_2 particle size in 2.5 %5A was around 44.9 nm (Table S. 4, Supplementary material). These results clearly show that the majority of Ru is located on the external surface of the

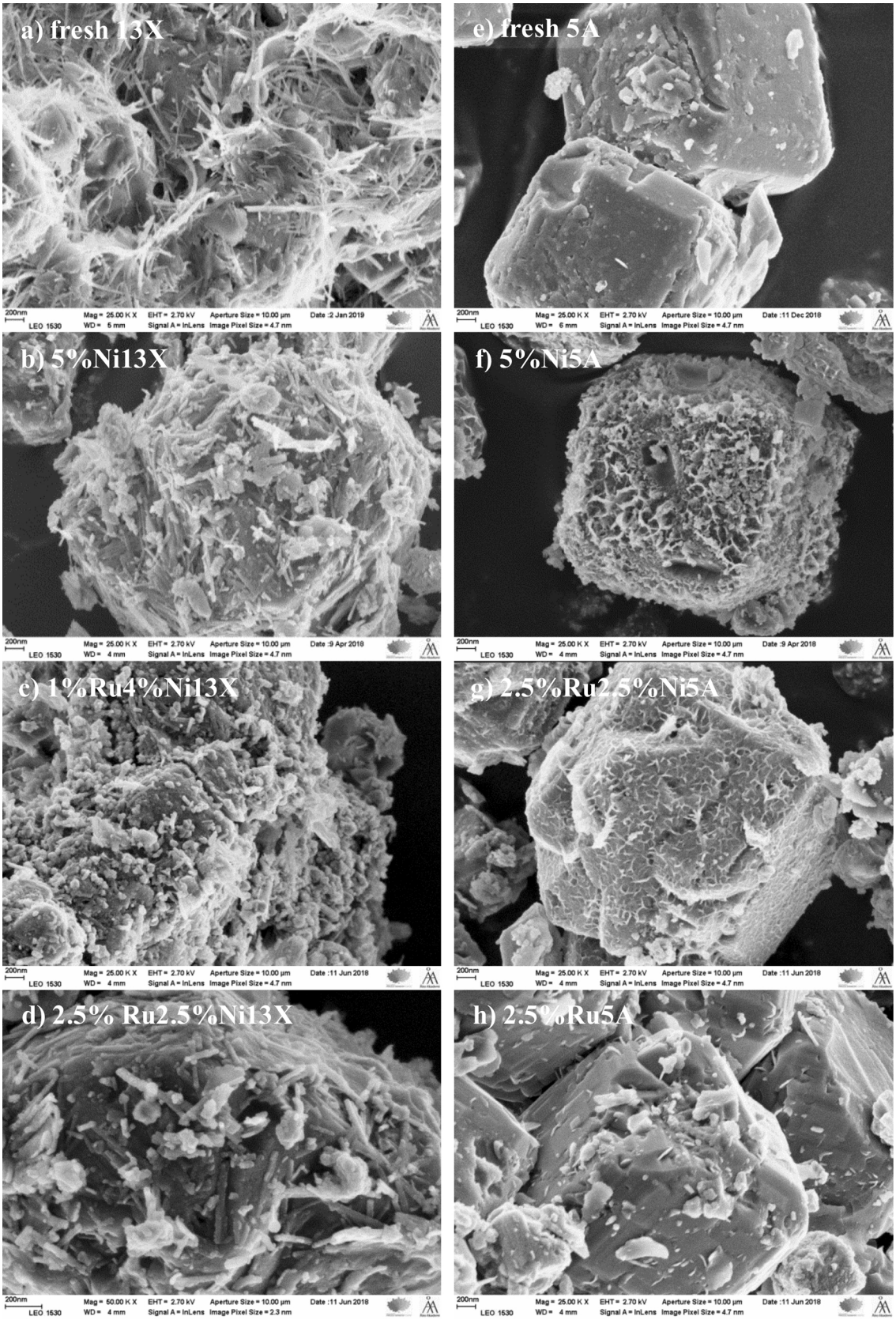

Fig. 2. SEM images of fresh 13X zeolite, fresh 5A zeolite and calcined catalysts, a) fresh 13X zeolite, b) 5%Ni13X, c)1%Ru4%Ni13X, d) 2.5 % Ru2.5 %Ni13X, e) fresh 5A zeolite, f) 5%Ni5A, g) 2.5 %Ru2.5 %Ni5A h) 2.5 %Ru5A.

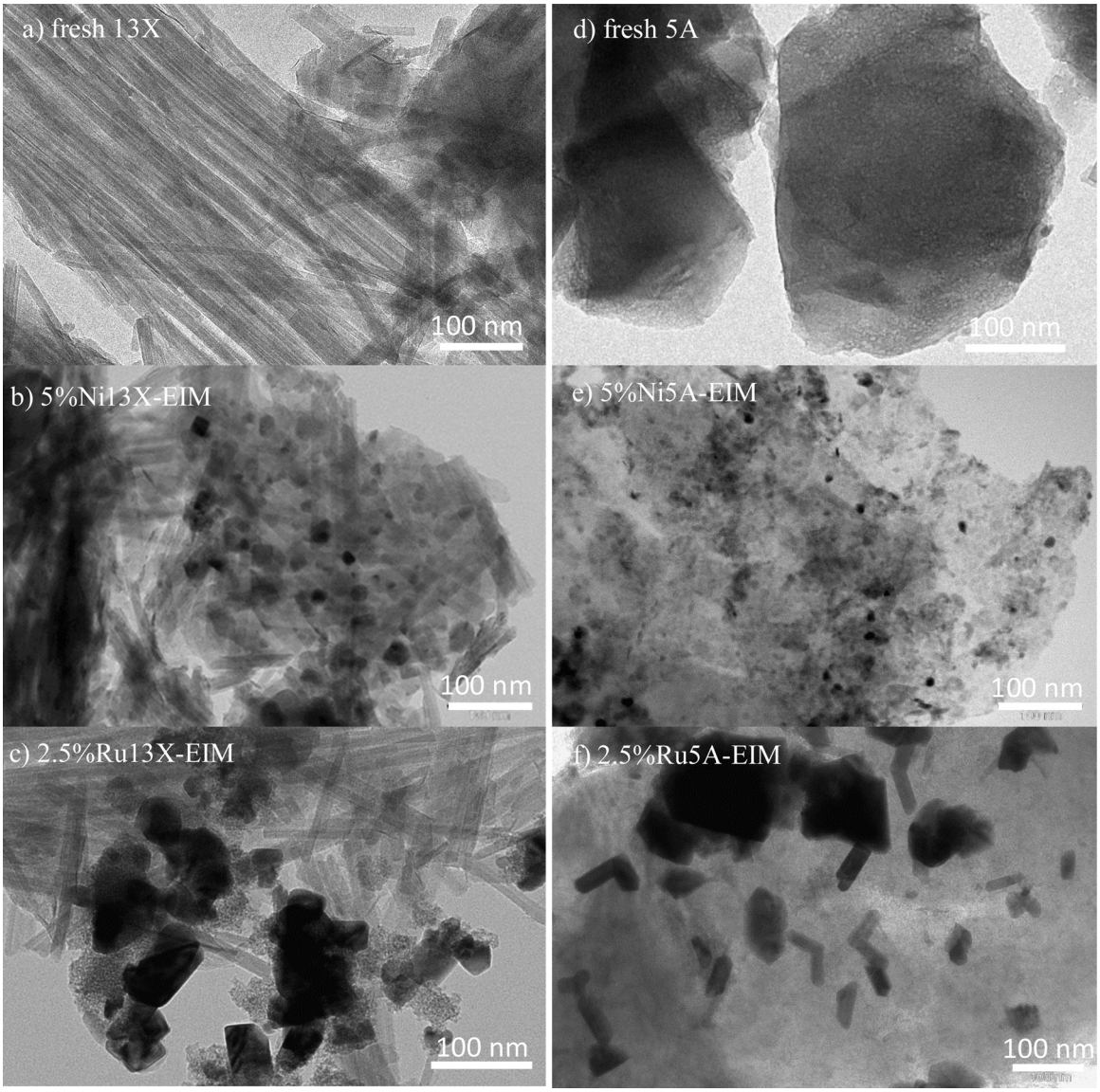

Fig. 3. TEM images of a) fresh 13X, b) 5%Ni13X, c) 2.5 %Ru13X, d) fresh 5A, e) 5%Ni5A and f) 2.5 %Ru5A.

zeolite particles.

3.1.4. STEM-EDX

TEM is a good method for investigating nanoparticle size in mono-metallic catalysts, however, in bi-metallic catalysts, it is unable to distinguish between the metals. Moreover, some very small nano NiO (RuO_2) particles invisible in TEM pictures, while these metal sites are always with high activity in reaction since their high surface free energy [26]. For this purpose, STEM assisted with EDX was employed for studying the Ni-Ru catalysts.

The STEM images, Na (gold), Ca (blue), and Ni (red) maps of 5% Ni13X, 2.5 %Ru2.5 %Ni13 × 5%Ni5A and 2.5 %Ru2.5 %Ni5A are shown in Fig. 4. As can be seen from the images, Ni dispersed well on 13X zeolite even on the bi-metallic catalysts prepared by evaporation impregnation. However, Ni appeared to form a type of egg shell coating on zeolite 5A instead of penetrating evenly into the particles, and similar phenomenon can be seen when both Ru and Ni were loaded on 5A zeolite (2.5 %Ru2.5 %Ni5A). For the catalysts 2.5 %Ru2.5 %Ni13X and 2.5 %Ru2.5 %Ni5A, Ru nanoparticles are much bigger than Ni Similarly to the mono-metallic Ru catalysts, the presence of both metal precursors in the solution does not seem to enhance the dispersion of the metals (Ru-, Ni-) based on STEM-EDX.

3.1.5. Nitrogen physisorption

Nitrogen adsorption-desorption was used to determine the specific surface area and pore volume of fresh zeolite and the impregnated catalysts (Table S. 5, Supplementary material).

Fresh 13X zeolite has the highest surface area 655 m^2/g, which is followed by 1%Ru4%Ni13X (640 m^2/g). The surface area decreased after the Ni modification for both 5%Ni13X and 5%Ni5A. Also, the micro-pore volume changed after the Ni loading on the 13X and 5A zeolite, and 5%Ni13X catalyst has the lowest micro-pore volume. The plausible reason for the decreasing of surface area and micropore volume is the blocking of micropores with NiO particles during the calcination step.

3.1.6. Temperature programed reduction

The H_2-Temperature programed reduction (H_2-TPR) profiles are shown in Fig. 5 for 13X, 5%Ni13X, 1%Ru4%Ni13X, 2.5 %Ru2.5 % Ni13X, 2.5 %Ru13X, fresh 5A zeolite, 5%Ni5A, 1%Ru4%Ni5A, 2.5 % Ru2.5 %Ni5A and 2.5 %Ru5A.

As can be seen from Fig. 5, a strong and broad peak can be observed at around 420 °C for the catalyst 5%Ni13X, which should correspond to the NiO particles in the super cages or on the surface of 13X zeolite [27,28]. Some nickel hydroxyaqua complexes may also be generated in

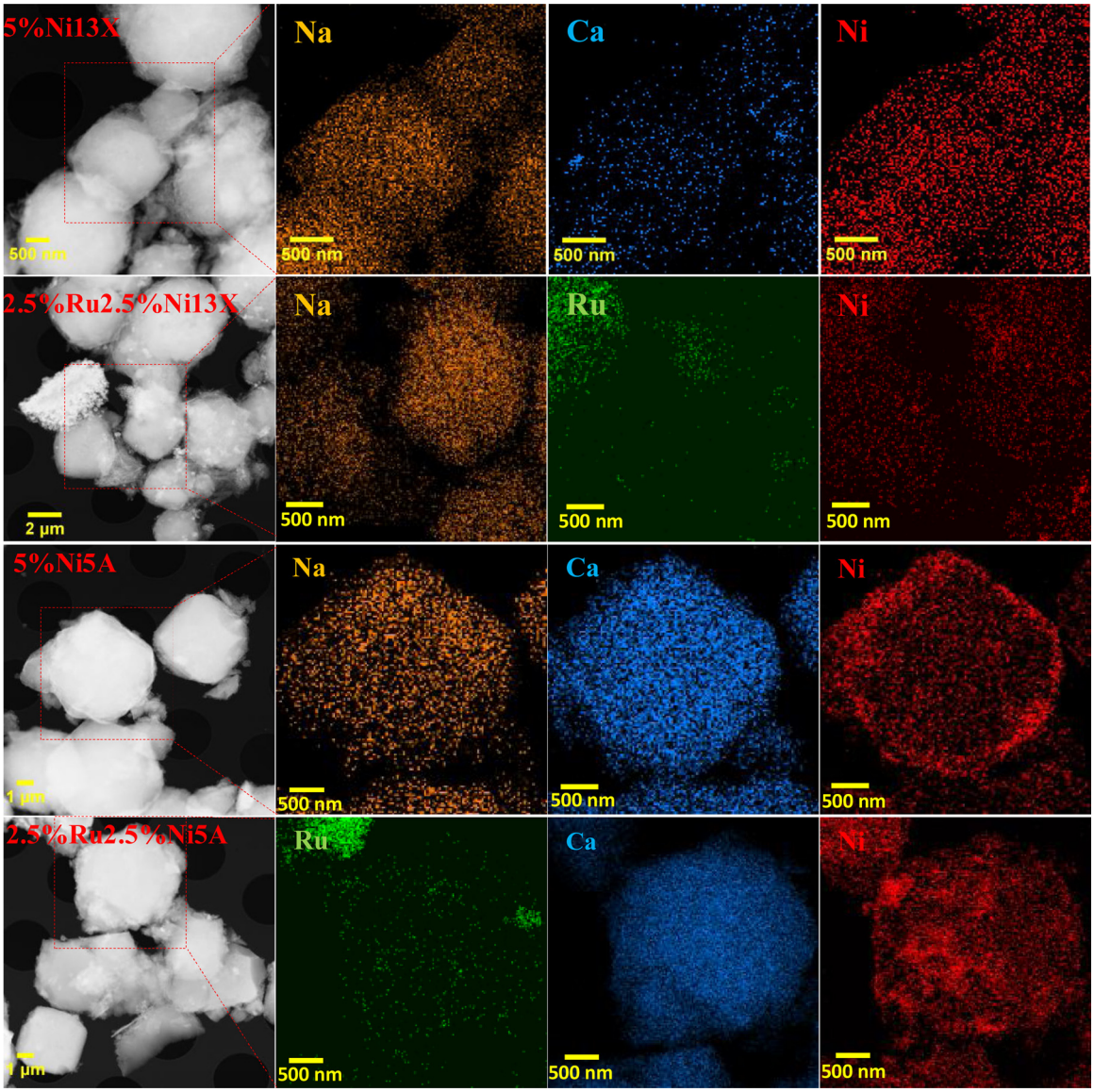

Fig. 4. STEM images (first row), Na (gold), Ca (light blue), Ru(green) and Ni (red) maps of 5%Ni13X, 2.5 %Ru2.5 %Ni13 × 5%Ni5A and 2.5 %Ru2.5 %Ni5A. (For interpretation of the references to colour in this figure legend, the reader is referred to the web version of this article).

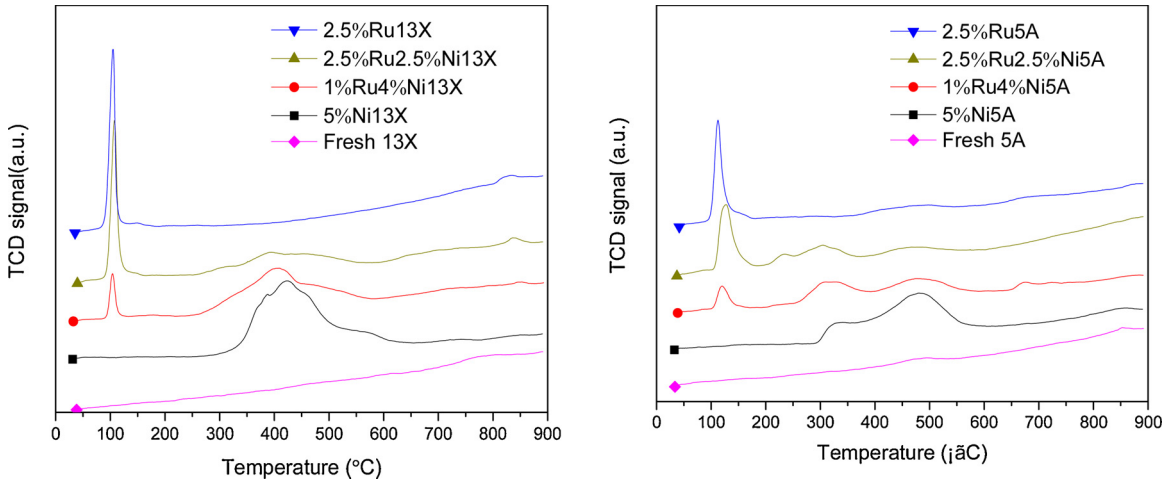

Fig. 5. H_2-TPR profiles of fresh 13X zeolite, 5%Ni13X, 1%Ru4%Ni13X, 2.5 %Ru2.5 %Ni13X, 2.5 %Ru13X, fresh 5A zeolite, 5%Ni5A, 1%Ru4%Ni5A, 2.5 %Ru2.5 %Ni5A, 2.5 %Ru5A.

the solution during catalysts preparation [29–31], which do not penetrate the pores of 13X zeolite as sufficiently leaving some of the NiO on or close to the surface of the particles. By contrast, two obvious peaks (at around 325 °C and 475 °C) were observed for 5%Ni5A, which should correspond to the NiO particles on the 5A zeolite surface and in the super cages, respectively.

After the introduction of Ru, a strong and sharp reduction peak could be observed at around 100 °C, Since NiO was reduced around 420 °C for 5%Ni13X as seen in Fig. 5, it can be deduced that ruthenium oxide on or in 13X zeolite with a low reduction temperature (around 100 °C). Moreover, NiO reducibility seemed to be enhanced by Ru oxide as the NiO reduction peaks can be observed to be shifted to lower temperatures in Fig. 5, when Ru was introduced. This shows clear interaction between the two metal phases directly or via the support [32,33]. Similarly, a sharp and strong RuO_2 reduction peak can be observed at around 120 °C for 1%Ru4%Ni5A, 2.5 %Ru2.5 %Ni5A and 2.5 %Ru5A zeolite catalysts. The H_2-TPR results provided important information of catalyst reduction temperature before using them in experiments.

3.1.7. Temperature programmed desorption of ammonia (NH_3-TPD)

NH_3-TPD was used to determine the acidic properties (weak, mild, strong) of 13X, 5A zeolite and Ru, Ni modified catalysts. For fresh 13X zeolite, peaks at around 175 °C and 625 °C can be found, which correspond to the weak (175 °C) and strong (625 °C) acidity, respectively [34–36]. With the ruthenium catalysts, a very sharp peak could be observed at around 290 °C. The introduction of Ni broadened the peak between 200 °C–400 °C and additional, peaks were observed at higher temperatures between 500 °C–600 °C, which indicate the presence of strong acid sites. However, the peaks at the higher temperatures were observed by the introduction of Ru, which indicates interaction between the metals and the support in the formation of acid sites into the catalyst. The ratio of O:Al:Si was, however, kept constant as displayed in the EDX results in Table S. 3 (Supplementary material).

The catalyst acidity distribution is shown in Fig. 6. With 13X zeolite, the introduction of Ni resulted in a clear increase in strong acid sites. In the bi-metallic catalysts, increasing amounts of Ru decreased both the concentration of strong acid sites and total acidity. The mono-metallic Ru catalyst displayed the lowest overall and strong acidity.

With 5A zeolite, the introduction of Ni resulted in a clear increase in strong acid sites, just as with 13 × . The introduction of Ru decreased again the concentration of strong acid sites, however, the trend in the total acidity was not as clear as with 13X, as ruthenium seemed to increase the concentration of weak acid sites.

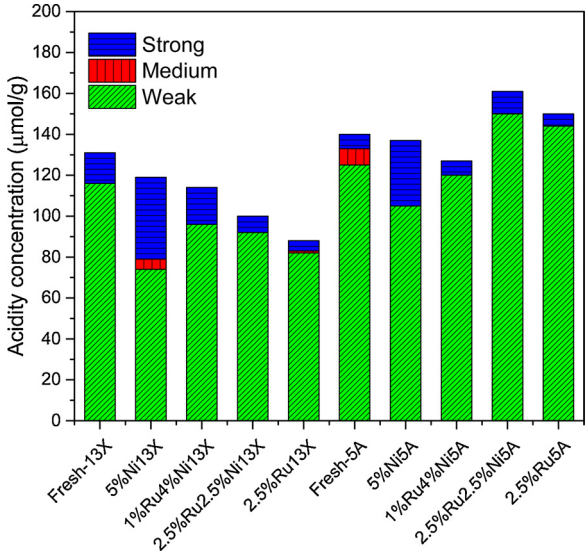

Fig. 6. The catalyst acidity distribution calculated based on the results of NH_3-TPD.

3.2. Results of CO_2 methanation reaction in a fixed bed reactor

3.2.1. Catalyst activity and selectivity

The catalyst activity and selectivity test were carried out in a lab scale fixed bed reactor system. The CO_2 conversion curves along with the selectivities towards CH_4 are shown in Figs. 7 and 8. Because the zeolites were already saturated with water at steady state condition when activity and selectivity data was recorded, adsorption enhancement can be excluded. It can be seen that conversion curves show similar trend, which increases strongly with increasing temperature to reach equilibrium values at the highest temperature. The results show that the choice of catalyst amount and GHSV was successful as a broad range of conversions was obtained, which enables good comparison of the catalysts performance.

Interestingly, the performance of the catalysts on the different zeolites was rather different. With 13X, the highest conversion were obtained with the mono-metallic Ni and Ru catalysts, with Ni out performing Ru at the lower temperatures. The bi-metallic catalysts did not perform as well, especially at the higher temperatures. The highest CH_4 selectivity was obtained with the mono-metallic Ru catalyst, while pure Ni on 13X as well as the bi-metallic catalyst displayed significantly lower selectivity, especially at the lower temperatures. The selectivities increased with temperature.

With 5A, the highest conversions were obtained with Ni on 5A, the conversions decrease with increasing loading of Ru. The selectivities of the 5A supported catalysts displayed almost opposite behaviors compared to the 13X supported catalysts. The lowest selectivity was obtained with Ru on 5A and selectivity increased with a decrease in Ru concentration and an increase in Ni concentration. Moreover, the highest selectivities were obtained at the lowest temperatures.

The differences in the behavior of the catalyst depending on the zeolites and the deposited metals are very interesting, as is the fact that the deposition of Ru did not increase the activity of the catalysts as expected [ref] (Figs. 7 & 8). Catalyst behavior and as a result also the formed reaction intermediates can vary depending not only on the type of the metal but also on the metal/support ratio and interaction, as well as reaction conditions and catalyst morphology. The reaction conditions were identical for all the tested catalysts. The activity on 13X decreased with increasing weak acidity (Fig. 6) and the same can be observed for 5A supported catalysts. This would indicate that too concentrated Lewis acidity is not favorable. However, the significant variations especially in the selectivity are most likely not dependent on the variations in acidity. The possible and plausible influence of the different factors explaining the observed results are presented below.

3.2.1.1. Reaction mechanisms of CO_2 hydrogenation on Ni and Ru. The reaction pathways of CO_2 methanation are divided into two main categories. The first one proposes the conversion of CO_2 to CO through reactive CO_2 adsorption via the reverse water gas shift reaction, and its subsequent reaction to methane through the same pathway as CO methanation [37,38]. The second pathway proposes dissociative adsorption of CO_2 followed by direct methanation [39,40]. Nowadays, it is generally accepted for most catalysts that in CO_2 methanation, CO is the main intermediate. The different reaction pathways also result in different rate limiting steps.

When evaluating the possible reaction mechanism depending on the metal, the probability of dissociative chemisorption on the surface is key as the second mechanism is based on it. The dissociative chemisorption energy of CO_2 on various metals was thoroughly described by T. Bligaard et al. [41]. The results show that dissociative chemisorbed of CO_2 occurs spontaneously on Ru with an energy of −0.77 eV. A value of 0.17 eV was obtained for the adsorption of CO_2 on Ni, which clearly shows that this pathway is not favorable and the first

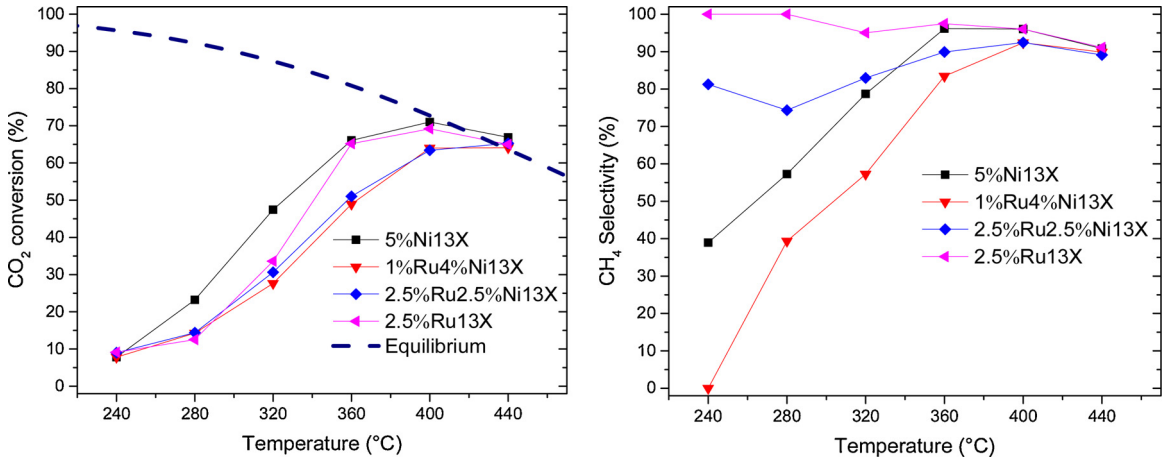

Fig. 7. CO_2 conversion and CH_4 selectivity with catalyst 5%Ni13X, 1%Ru4%Ni13X, 2.5 %Ru2.5 %Ni13X and 2.5 %Ru13X (reduction at 500 °C, 4 h) 0.9 g, 150 mL/min He, 40 mL/min H_2, 10 mL/min CO_2.

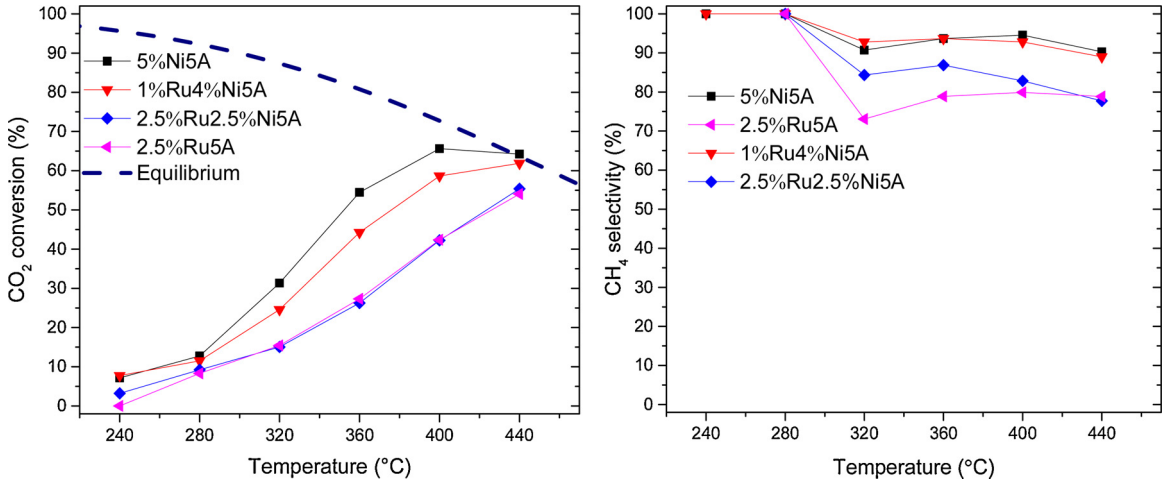

Fig. 8. CO_2 conversion and CH_4 selectivity with 1%Ru4%Ni5A, 2.5 %Ru2.5 %Ni5A and 2.5 %Ru5A (reduction at 500 °C, 4 h) 0.9 g, 150 mL/min N_2, 40 mL/min H_2, 10 mL/min CO_2.

mechanism seems more likely.

Westermann et al. [42] studied the reaction mechanism of CO_2 methanation using nickel impregnated on ultra stable Y zeolite with IR measurements. They detected both carbonate and formate species on the Ni, but concluded that the CO_2 methanation pathway does not proceed through carbonate formation but through formate dissociation on Ni, leading to the formation of adsorbed CO. They concluded that CO is the main intermediate and its dissociation is the rate determining step of CO_2 methanation. The reaction pathway via formate formation was also recently reported by Dongapure et al. for Ni/Al_2O_3 [43]. Detailed studies regarding the interaction of CO_2 with Ni(110) via high pressure TPR (Temperature Programed Reactions) experiments were carried out by Vesselli et al. [44]. They reported that CO_2 chemisorbed on Ni(110) is negatively charged and that it is mainly bonded via the carbon atom. The molecule binds to the surface with a resulting energy barrier for its hydrogenation smaller than the energy barrier for CO_2 desorption or that for dissociation into COad and Oad. The presence of adsorbed and dissociated hydrogen Had leads to the formation of formate intermediates which subsequently react to provide methane.

They also performed ultrahigh vacuum (UHV) low temperature experiments and DFT calculations, which indicated that CO + OH is generated from CO2 hydrogenation via a type of Eley-Rideal mechanism (Eqs. 4 & 5) [44,45].

Based on the finding presented above, the CO_2 methanation on Ni is proposed to follow the following mechanism, where ad represents a surface cite/adsorbed species:

$$H2(g) + 2ad \leftrightarrow 2Had \quad (3)$$

$$CO_2(g) + Had \leftrightarrow HCOOad \quad (4)$$

$$HCOOad + Had \leftrightarrow H2Oad + COad \quad (5)$$

$$COad \leftrightarrow Cad + Oad \text{ (rate limiting step)} \quad (6)$$

$$Cad + Had \leftrightarrow CHad \quad (7)$$

$$CHad + Had \leftrightarrow CH2ad \quad (8)$$

$$CH_2ad + Had \leftrightarrow CH3ad \quad (9)$$

$$CH_3ad + Had \leftrightarrow CH4ad \quad (10)$$

$$CH_4ad \leftrightarrow CH_4(g) \quad (11)$$

$$Oad + Had \leftrightarrow OHad \quad (12)$$

$$OHad + Had \leftrightarrow H2Oad \quad (13)$$

$$H_2Oad \leftrightarrow H_2Og \quad (14)$$

Reaction intermediates in CO_2 methanation when using ruthenium supported on alumina ($Ru/\gamma\text{-}Al_2O_3$) as catalysts were investigated by [37] Eckle et al., 2011. The intermediates were investigated by steady state isotopic transient kinetic analysis coupled with DRIFT

experiments. The formate mechanism was considered highly unlikely to be the dominant rate determining reaction. It was proposed that on a Ru catalyst, CO_2 methanation proceeds via dissociative adsorption (Eq. (15)) forming COad and Oad, which is the rate determining reaction of the process. Based on the results presented above, the reaction mechanism can be presented as

$$CO_2 \leftrightarrow COad + Oad \text{ (rate determining step)} \quad (15)$$

$$COad \leftrightarrow Cad + Oad \text{ (rapid)} \quad (16)$$

followed by reactions (7)–(14).

Based on the reaction mechanisms and the literature data presented above, it could be argued that the higher selectivity achieved with Ru is due to the efficient CO dissociation which minimized the desorption of CO. However, the reaction mechanisms cannot explain the very significant increase of selectivity observed with increasing temperature and conversion for Ni on 13X and the opposite behavior for Ni and Ru on 5A (Figs. 7 & 8). Catalyst behavior and as a result also the formed reaction intermediates can vary depending not only on the type of the metal but also other factors and partly contradicting observations have been reported in literature.

3.2.1.2. Differences in characteristics of the support. Both zeolites were primarily chosen for their large water adsorption capacity in order to obtain the bi-functional catalytic and water adsorptive capabilities of the catalysts. However, there exist some differences between them. Zeolite 13X has a higher water adsorption capacity compared to 5A. When increasing the experimental temperature towards 400 °C, the water is mostly desorbed from both [46]. The zeolites adsorb also efficiently CO_2 and the capacity of 5A is higher compared to 13 ×. Both zeolites also adsorb rather efficiently CH_4 and CO [46,47].

The adsorption of the different compound is at least partly competitive and e.g. a lower amount of water enables the increased loading of CO_2. It has been reported that an increased amount of methane decreases the CO2 uptake for 5A, whereas 13X would not be so significantly influenced [46,48].

The high concentration of the reactant CO_2 on the zeolite and close to the reactive sites is logically beneficial for the reaction, whereas the high concentration of the final product CH_4 could have a negative effect on the reaction rate, as well as promote side product (CO) formation. This could contribute to the decreasing selectivity of the ruthenium catalysts on both zeolites with increasing conversion.

3.2.1.3. Morphology of the catalyst. The pore size of zeolite 5A is about 5 Å whereas the pore size of 13 X is about 10 Å [11]. As described previously in the results part, the nanoparticle size of Ru was much larger compared to Ni in both the mono- and bi-metallic catalysts. The Ni nanoparticle size was significantly smaller compared to Ru in all the catalysts. Well below one nm particles were observed for Ni, while the Ru nanoparticles were much larger (Table S4.) also in average size. When considering the pore sizes of the zeolites, it is evident that the ruthenium was deposited on both zeolites as an eggshell structure, as was the nickel on zeolite 5A. However, a part of the nickel was able to penetrate the pores of the zeolite forming highly active sub-nano sized nanoparticles. This was displayed in the nitrogen physisorption results (Table S. 5), as the total surface area and total pore volume of 5%Ni13X were about 45 % lower compared to pristine 13X, while the values did not change significantly for the Ru containing catalysts compared to the pristine zeolites. As described previously in the experimental section, the zeolites were saturated with water during the steady state experiments. This leads to the fact that the concentration of water inside the pores of the zeolites was very high at the lower experimental temperatures, whereas, at the higher temperatures, the majority of water was desorbed. The high concentration of water promoted the formation of the intermediary product CO decreasing the selectivity according to the overall reaction (Eqs. 3–14) [11]. With 13X zeolite, the highest conversions were obtained with the single metal catalysts. This explains why the Ni / 13X catalysts where the most active sub-nano sized nanoparticles were inside the water containing pores of the zeolite, displayed increasing selectivity with temperature. On the contrary, the ruthenium was located on the outer surface of the zeolite 13X, which is why the active external sites were not influenced by the water retained inside the zeolite and high selectivity was observed even at lower temperature. With zeolite 5 A, both Ni and Ru displayed high selectivity at lower temperature as both formed an eggshell structure.

The intended advantage of obtaining close proximity of the reactive sites on the sub-nano Ni nanoparticles with the water adsorbing sites inside 13 X acts as a disadvantage in steady state experiments in decreased selectivity, even though high activity is maintained. The more robust eggshell structure, where the reactive sites are located further from the water adsorbing sites located inside the zeolites do not suffer as much from this disadvantage. However, it must be pointed out that this applies to steady state conditions and not the dynamic conditions the bi-functional catalyst is intended to be operated in.

3.2.2. Catalyst stability

The catalyst stability test was carried out at 360 °C for 200 h, and the catalysts were reduced at 500 °C for 4 h prior to performing the catalyst evaluation experiments. The CO_2 conversions are shown in Fig. 9. Very stable performance can be observed for both catalysts. It can be concluded that the stability of the catalysts was excellent with

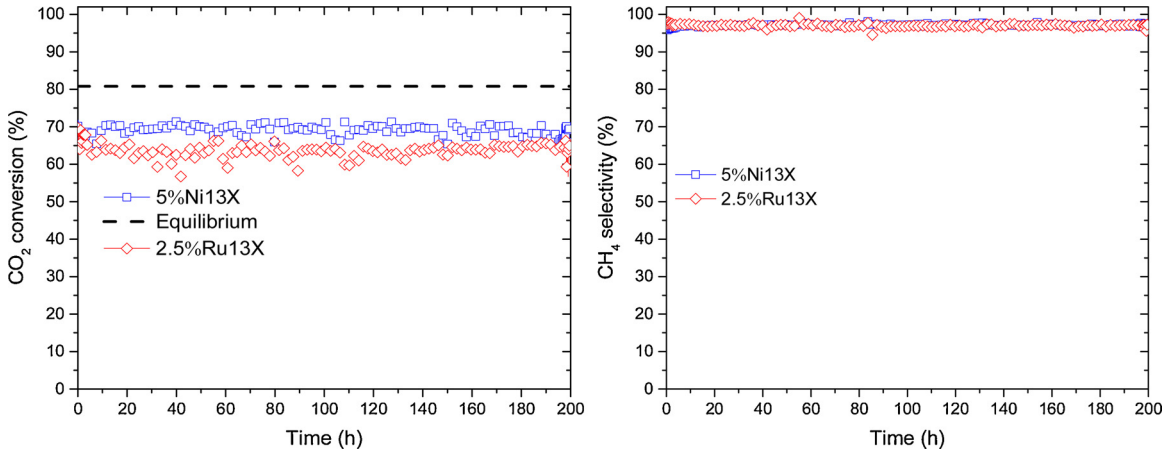

Fig. 9. CO_2 conversion and CH_4 selectivity with catalyst 5%Ni13X and 2.5 %Ru13X (reduction at 500 °C, 4 h), 0.9 g, 150 mL/min N_2, 40 mL/min H_2, 360 °C, 10 mL/min CO_2 during 200 h experiments.

time on stream and no indications of deactivation could be observed.

4. Conclusions

Nickel-ruthenium modified mono- and bi-metallic catalysts were synthesized on zeolite 13X and 5A using evaporation impregnation. The physico-chemical properties of the pristine and modified catalysts were characterized using XRD, SEM-EDX, TEM, STEM-EDX, N_2 physisorption and TPD-NH_3. The catalysts were tested for CO_2 methanation in a fixed bed reactor system in the temperature interval $240-440\,^{\circ}C$.

The surface area and, micro-pore volume decreased after Ni modification of 13X zeolite, however, no significant influence was observed with 5A. A significantly smaller cluster size was obtained for Ni while Ru formed large nanoparticles. The same observation was valid for both mono- and bi-metallic catalysts. The metal modification clearly influenced the acidity of the catalysts with Ni promoting strong acidity.

The 13X supported catalyst outperformed in general the 5A supported ones, when considering conversion. Interestingly, the conversion and selectivity depended significantly on the zeolite. With 13X, the highest conversions were obtained with the mono-metallic catalysts, while with 5A, the conversion decreased with increasing Ru loading. With 13X, the highest selectivity was obtained with pure Ru catalyst, while with 5A, the result was opposite. Moreover, with 13X the selectivity increased with temperature, while with 5A, it was the opposite.

The selectivity was clearly influenced by the fact that Ni was able to penetrate the pores of the 13X catalyst, while the Ru nanoparticles were formed on the surface of the particles. This was also the case with both Ni and Ru on 5A. This resulted in the active Ni clusters inside 13X being influenced by the high concentration of water inside the zeolite at lower temperatures, while at higher temperature, water was desorbed from the catalyst which resulted in increased selectivity. With the egg shell type structure for Ru/13X and Ni/Ru/5A, the water adsorbed by the zeolite did not influence selectivity as it was not in such close proximity to the active sites. Moreover, the selectivity was most probably influenced by the competitive adsorption of CO_2 and methane in 5A as well as the different reaction mechanisms of the methanation on the Ni and Ru metals. The catalysts exhibited good stability and CH_4 selectivity during 200 h.

It can be concluded that the CO_2 methanation by Ni based catalysts cannot be improved by adding Ru. However, the selectivity can be significantly influenced depending on the properties of 13X and 5A zeolites.

CRediT authorship contribution statement

Liangyuan Wei: Conceptualization, Software, Investigation, Formal analysis, Data curation, Visualization, Writing - original draft. **Narendra Kumar:** Methodology, Investigation, Formal analysis, Resources, Supervision, Writing - review & editing. **Wim Haije:** Conceptualization, Investigation, Methodology, Supervision, Writing - review & editing. **Janne Peltonen:** Investigation. **Markus Peurla:** Investigation. **Henrik Grénman:** Conceptualization, Methodology, Resources, Supervision, Project administration, Funding acquisition, Writing - review & editing. **Wiebren de Jong:** Resources, Supervision, Writing - review & editing.

Declaration of Competing Interest

The authors declare that they have no known competing financial interests or personal relationships that could have appeared to influence the work reported in this paper.

Acknowledgments

The research work is a part of the activities of large scale energy storage group (process and energy department) in Delft University of Technology and Johan Gadolin Process Chemistry Centre, a centre of excellence financed by Åbo Akademi University. The authors acknowledge the financial support from Åbo Akademi University, The Finnish Society of Science and Letters for Liangyuan's visiting at Turku, and the support for the catalyst preparation, characterization and testing. The authors acknowledge the PhD scholarship awarded to Liangyuan Wei by the China Scholarship Council.

Appendix A. Supplementary data

Supplementary material related to this article can be found, in the online version, at doi:https://doi.org/10.1016/j.mcat.2020.111115.

References

[1] W. De Jong, J. Re. Van Ommen, Biomass, A Sustainable Energy Source for the Future – Fundamentals of Conversion Processes, John Wiley & Sons, New York (USA), 2014.
[2] L. Wei, et al., Absorption-enhanced steam gasification of biomass for hydrogen production: effect of calcium oxide addition on steam gasification of pyrolytic volatiles, Int. J. Hydrogen Energy 39 (28) (2014) 15416–15423.
[3] H.J. Pasman, W.J. Rogers, Risk assessment by means of Bayesian networks: a comparative study of compressed and liquefied H2 transportation and tank station risks, Int. J. Hydrogen Energy 37 (22) (2012) 17415–17425.
[4] K. Mueller, W. Arlt, Status and development in hydrogen transport and storage for energy applications, Energy Technol. 1 (9) (2013) 501–511.
[5] T. Schaaf, et al., Methanation of CO_2-storage of renewable energy in a gas distribution system, Energy Sustain. Soc. 4 (1) (2014) 2.
[6] A. Poullikkas, A comparative overview of large-scale battery systems for electricity storage, Renew. Sustain. Energy Rev. 27 (Supplement C) (2013) 778–788.
[7] P. Frontera, et al., Supported catalysts for CO_2 methanation: a review, Catalysts 7 (2) (2017) 59.
[8] V.M. Lebarbier, et al., Sorption-enhanced synthetic natural gas (SNG) production from syngas: a novel process combining CO methanation, water-gas shift, and CO_2 capture, Appl. Catal. B 144 (1) (2013) 223–232.
[9] S. Walspurger, et al., Sorption enhanced methanation for substitute natural gas production: experimental results and thermodynamic considerations, Chem. Eng. J. 242 (2014) 379–386.
[10] R. Delmelle, et al., Development of improved nickel catalysts for sorption enhanced CO_2 methanation, Int. J. Hydrogen Energy 41 (44) (2016) 20185–20191.
[11] A. Borgschulte, et al., Sorption enhanced CO_2 methanation, J. Chem. Soc. Faraday Trans. 15 (24) (2013) 9620–9625.
[12] S. Rönsch, et al., Review on methanation - from fundamentals to current projects, Fuel 166 (2016) 276–296.
[13] W.A. Wan Abu Bakar, R. Ali, N.S. Mohammad, The effect of noble metals on catalytic methanation reaction over supported Mn/Ni oxide based catalysts, Arab. J. Chem. 8 (5) (2015) 632–643.
[14] J.J. Gao, et al., Recent advances in methanation catalysts for the production of synthetic natural gas, RSC Adv. 5 (29) (2015) 22759–22776.
[15] R.A. Hubble, J.Y. Lim, J.S. Dennis, Kinetic studies of CO_2 methanation over a Ni/γ-Al_2O_3 catalyst, Faraday Discuss. 192 (2016) 529–544.
[16] K. Jalama, Carbon dioxide hydrogenation over nickel-, ruthenium-, and copper-based catalysts: review of kinetics and mechanism, Catal. Rev. 59 (2) (2017) 95–164.
[17] T. Zhao, et al., Controllable preparation of ZIF-67 derived catalyst for CO2 methanation, Mol. Catal. 474 (2019) 110421.
[18] Y. Li, et al., Metal-foam-structured Ni-Al_2O_3 catalysts: wet chemical etching preparation and syngas methanation performance, Appl. Catal. A Gen. 510 (2016) 216–226.
[19] R.A. Hubble, J.Y. Lim, J.S. Dennis, Kinetic studies of CO_2 methanation over a Ni/gamma-Al_2O_3 catalyst, Faraday Discuss. 192 (2016) 529–544.
[20] M.A.A. Aziz, et al., CO_2 methanation over heterogeneous catalysts: recent progress and future prospects, Green Chem. 17 (5) (2015) 2647–2663.
[21] W. Wei, G. Jinlong, Methanation of carbon dioxide: an overview, Front. Chem. Sci. Eng. 5 (1) (2011) 2–10.
[22] W.A.W. Abu Bakar, R. Ali, S. Toemen, Catalytic methanation reaction over supported nickel–ruthenium oxide base for purification of simulated natural gas, Sci. Iran. 19 (3) (2012) 525–534.
[23] E.-P. Ng, S. Mintova, Nanoporous materials with enhanced hydrophilicity and high water sorption capacity, Microporous Mesoporous Mater. 114 (1) (2008) 1–26.
[24] S. Abelló, C. Berrueco, D. Montané, High-loaded nickel–alumina catalyst for direct CO_2 hydrogenation into synthetic natural gas (SNG), Fuel 113 (2013) 598–609.
[25] S. Abate, et al., Synthesis, characterization, and activity pattern of Ni–Al hydrotalcite catalysts in CO_2 methanation, Ind. Eng. Chem. Res. 55 (30) (2016) 8299–8308.
[26] X.F. Yang, et al., Single-atom catalysts: a new frontier in heterogeneous catalysis,

Acc. Chem. Res. 46 (8) (2013) 1740–1748.
[27] A. Luengnaruemitchai, A. Kaengsilalai, Activity of different zeolite-supported Ni catalysts for methane reforming with carbon dioxide, Chem. Eng. J. 144 (1) (2008) 96–102.
[28] I. Graça, et al., CO_2 hydrogenation into CH_4 on NiHNaUSY zeolites, Appl. Catal. B 147 (Supplement C) (2014) 101–110.
[29] B.-H. Chen, et al., Towards a full understanding of the nature of Ni(ii) species and hydroxyl groups over highly siliceous HZSM-5 zeolite supported nickel catalysts prepared by a deposition–precipitation method, J. Chem. Soc. Dalton Trans. 45 (6) (2016) 2720–2739.
[30] P. Burattin, M. Che, C. Louis, Molecular approach to the mechanism of deposition − precipitation of the Ni (II) phase on silica, J. Phys. Chem. B 102 (15) (1998) 2722–2732.
[31] R. Nares, et al., Ni/H beta-zeolite catalysts prepared by deposition-precipitation, J. Phys. Chem. B 106 (51) (2002) 13287–13293.
[32] S. Tada, et al., Study of $RuNi/TiO_2$ catalysts for selective CO methanation, Appl. Catal. B 140–141 (2013) 258–264.
[33] M. Kimura, et al., Selective methanation of CO in hydrogen-rich gases involving large amounts of CO_2 over Ru-modified Ni-Al mixed oxide catalysts, Appl. Catal. A Gen. 379 (1) (2010) 182–187.
[34] D. Jin, et al., Microwave assisted in situ synthesis of USY-encapsulated heteropoly acid (HPW-USY) catalysts, Appl. Catal. A Gen. 352 (1) (2009) 259–264.
[35] F. Arena, R. Dario, A. Parmaliana, A characterization study of the surface acidity of solid catalysts by temperature programmed methods, Appl. Catal. A Gen. 170 (1) (1998) 127–137.
[36] F. Lónyi, J. Valyon, On the interpretation of the NH_3-TPD patterns of H-ZSM-5 and H-mordenite, Microporous Mesoporous Mater. 47 (2) (2001) 293–301.
[37] D. Peebles, et al., Methanation of carbon dioxide on nickel(100) and the effects of surface modifiers, J. Phys. Chem. 87 (1983) 4378–4387.
[38] S. Eckle, S. Eckle, H.G. Anfang, R.J. Behm, et al., Reaction intermediates and side products in the methanation of CO and CO2 over supported Ru catalysts in H2-rich reformate gases, J. Phys. Chem. C 2011 (115) (2011) 1361–1367.
[39] G. Mills, F. Steffgen, Catalytic methanation, Catal. Rev. 8 (1974) 159–210.
[40] S. Sharma, et al., CO2 methanation on Ru-doped ceria, J. Catal. (2011) 297–309.
[41] T. Bligaard, et al., The Brønsted–Evans–Polanyi relation and the volcano curve in heterogeneous catalysis, J. Catal. 224 (2004) 206–217.
[42] A. Westermann, et al., Insight into CO2 methanation mechanism over NiUSY zeolites: An operando IR study, Appl. Catal. B 174–175 (2015) 120–125.
[43] P. Dongapure, et al., Variations in Activity of Ru/TiO2 and Ru/Al2O3 Catalysts for CO2 Hydrogenation: an Investigation by In-Situ Infrared Spectroscopy Studies, Molecular Catalysis, (2020), p. 110700.
[44] E. Vesselli, et al., Carbon dioxide hydrogenation on Ni(110), J. Am. Chem. Soc. 130 (2008) 11417–11422.
[45] M. Roiaz, et al., Reverse water–gas shift or sabatier methanation on Ni(110)? Stable surface species at near-ambient pressure, J. Am. Chem. Soc. 138 (2016) 4146–4154.
[46] Y. Wang, M. Douglas LeVan, Adsorption equilibrium of carbon dioxide and water vapor on zeolites 5A and 13X and silica gel: pure components, J. Chem. Eng. Data 54 (10) (2009) 2839–2844.
[47] P. Rodilnak, R. Kobayashi, Adsorption of methane and several mixtures and carbon dioxide at elevated pressures and near ambient temperatures on 5A and 13X molecular sieves by tracer perturbation chromatography, AIChE J. 26 (4) (1980) 616–625.
[48] T. Montanari, et al., CO2 separation and landfill biogas upgrading: a comparison of 4A and 13X zeolite adsorbents, Energy 36 (2011) 314–319.